RSC Advances

PAPER

View Article Online
View Journal | View Issue

Check for updates

Cite this: *RSC Adv.*, 2023, **13**, 32433

Synthesis of 3-hydroxypyridin-4-one derivatives bearing benzyl hydrazide substitutions towards anti-tyrosinase and free radical scavenging activities†

Bahareh Hassani,‡[a] Fateme Zare,‡[b] Leila Emami,[b] Mehdi Khoshneviszadeh,[a] Razieh Fazel,[a] Negin Kave,[a] Razieh Sabet *[a] and Hossein Sadeghpour*[a]

Received 23rd September 2023
Accepted 10th October 2023

DOI: 10.1039/d3ra06490e

rsc.li/rsc-advances

Tyrosinase is a vital enzyme in the biosynthesis of melanin, which has a significant role in skin protection. Due to the importance of the tyrosinase enzyme in the cosmetics and health industries, studies to design new tyrosinase inhibitors have been expanded. In this study, the design and synthesis of 3-dihydroxypyridine-4-one derivatives containing benzo hydrazide groups with different substitutions were carried out, and their antioxidant and anti-tyrosinase activities were also evaluated. The proposed compounds showed tyrosinase inhibitory effects (IC_{50}) in the 25.29 to 64.13 μM range. Among all compounds, **6i** showed potent anti-tyrosinase activity with an IC_{50} = 25.29 μM. Also, the antioxidant activity of derivatives by using DPPH radical scavenging indicates an EC_{50} value between 0.039 and 0.389 mM. Molecular docking studies were performed to reveal the position and interactions of **6i** as the most potent inhibitor within the tyrosinase active site. The results showed that **6i** binds well to the proposed binding site and forms a stable complex with the target protein. Furthermore, the physicochemical profiles of the tested compounds indicated drug-like and bioavailability properties. The kinetic assay revealed that **6i** acts as a competitive inhibitor. Also, for the estimation of the reactivity of the best compound (**6i**), the density functional theory (DFT) was performed at the B3LYP/6-31+G** .

Open Access Article. Published on 07 November 2023. Downloaded on 2/8/2026 4:49:23 PM.
This article is licensed under a Creative Commons Attribution-NonCommercial 3.0 Unported Licence.

1. Introduction

Tyrosinase is a copper-containing enzyme that plays an important role in melanin formation *via* mono- and di-phenolase reactions.[1] Melanin can prevent ultraviolet skin damage; on the other hand, excessive gathering of melanin leads to different skin discomforts, such as age spots, malignant melanoma, and melisma.[2] Tyrosinase is responsible for the undesirable enzymatic browning of fruits and vegetables.[3] Various tyrosinase inhibitors have been established today, but due to the different side effects of available tyrosine inhibitor agents, drug design and studies on this enzyme are necessary.[4] So far, several natural and synthetic inhibitors for tyrosinase enzymes have been identified.[5–8] The studies showed that the compounds can inhibit tyrosinase enzyme in several different ways, including reduction of dopaquinone to dopa (ascorbic acid),[9] reduction of the amount of dopaquinone (thiol analogs),[10] and much greater affinity to tyrosinase enzyme compared to the main substrate (phenolic compounds).[11] Also, the alteration in the shape of the active site of the enzyme, such as compounds with acidic or basic properties,[12] the inactivation of the enzyme through the covalent bond with the enzyme, and irreversible inhibition of the enzyme,[13] and finally, the occupation of the active site and reversible inhibition of the enzyme[14] are the other mechanisms of tyrosinase inhibition. In recent years, researchers have focused more on synthesizing compounds with a phenolic group,[15] which showed more affinity to the tyrosinase enzyme than dopaquinone and inhibited melanin formation.[15] One of the scaffolds that has received much attention from researchers is hydroxypyridine (HP). The HPs are N-heterocycles bearing a hydroxyl and a ketone group. These scaffolds included three subgroups: 1, 2-HP, 3, 2-HP, and 3, 4-HP.[16] Due to their chelating properties, the 3,4-HP scaffolds were the more basic, and some of their derivatives are used in the clinic, such as diferiprone.[17] The derivatives of HPs can be easily synthesized and functionalized in different positions. Based on this fact, the hydroxypyridinone-like scaffolds (HPOs) were extensively used for research with various biological activities such as antiproliferative,[18] chelating

[a]*Department of Medicinal Chemistry, Faculty of Pharmacy, Shiraz University of Medical Sciences, Shiraz, Iran. E-mail: sabet_r@sums.ac.ir; Fax: +98-7132424126; Tel: +98-7132424127-8*

[b]*Faculty of Pharmacy and Pharmaceutical Sciences Research Center, Shiraz University of Medical Sciences, Shiraz, Iran. E-mail: sadeghpurh@sums.ac.ir; Fax: +98-7132424126; Tel: +98-7132424127-8*

† Electronic supplementary information (ESI) available. See DOI: https://doi.org/10.1039/d3ra06490e

‡ These authors are equally to this work.

© 2023 The Author(s). Published by the Royal Society of Chemistry

Open Access Article. Published on 07 November 2023. Downloaded on 2/8/2026 4:49:23 PM.
This article is licensed under a Creative Commons Attribution-NonCommercial 3.0 Unported Licence.

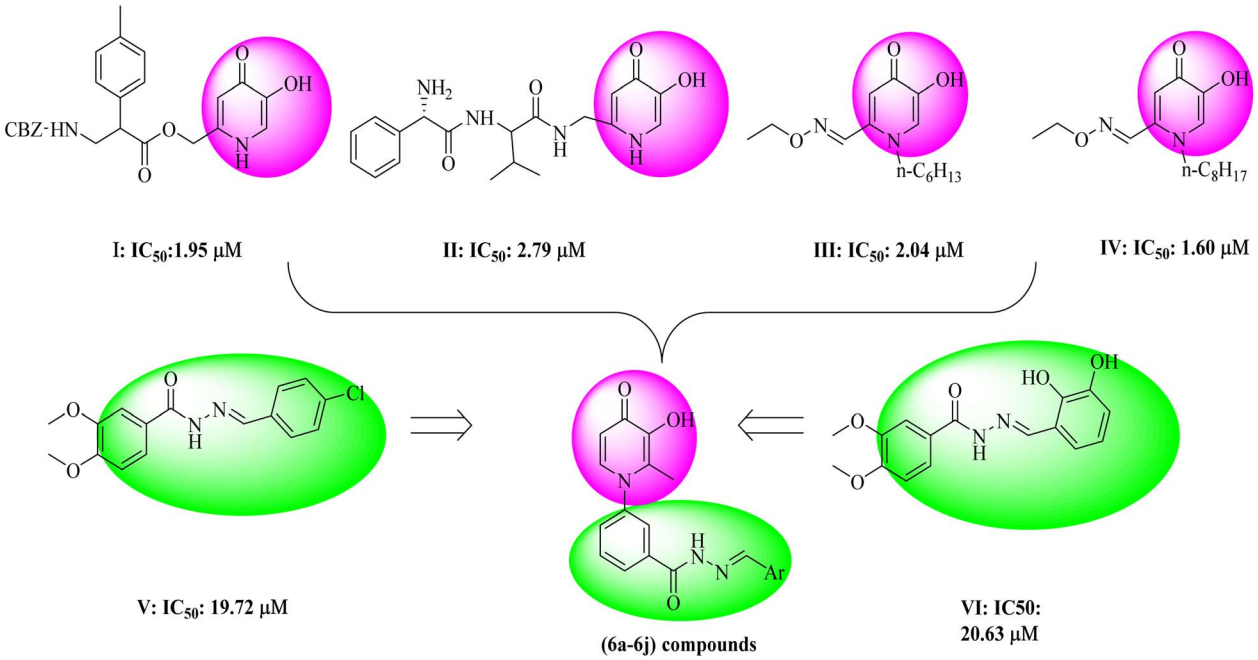

Fig. 1 The design approach of synthesized compounds.

agents,[19] antimicrobial,[20,21] monoamine oxidase,[22] and cytotoxic agents.[23] Due to their copper chelation ability, they were used as tyrosinase enzyme inhibitors.[24–26] In a recent study to search the possible application of hydroxypyridine (HP) as a tyrosinase inhibitor, some novel hydroxy pyridinone (compound I and II) was reported as tyrosinase inhibitors with IC_{50} = 1.95 μM and 2.79 μM against tyrosinase in diphenolase activity, respectively.[27] In 2016, hydroxypyridinone derivatives containing an oxime ether moiety (compound III and IV) were found to be another potent inhibitor with an IC_{50} value of 2.04 μM and 1.60 μM against monophenolase activity[28] (Fig. 1). On the other hand, in previous studies, the benzyl hydrazide group derivatives were synthesized with proper tyrosinase inhibitory potential (compounds V and VI) (Fig. 1).[29] Given the critical tyrosinase activities of 3-hydroxypyridine-4-one and benzyl hydrazide as tyrosinase inhibitors, we followed fragment-based hybridization of 3-hydroxypyridine-4-one and benzyl hydrazide groups to design a new series of tyrosinase inhibitors.

In the present work, the synthesis of some 3-hydroxypyridine-4-one benzyl hydrazide derivatives was assigned. The activity of these compounds as tyrosinase inhibitors was evaluated, and also antioxidant activity was examined. In addition, molecular docking studies were applied to understand the binding poses and interactions of compounds in the active site of the enzyme. The physicochemical properties of these compounds were also determined. As well as DFT calculations were applied to investigate the electronic structure of molecules.

2. Results and discussion

2.1 Chemistry

Synthesis of 3-hydroxypyridine-4-one benzyl-hydrazide derivatives was executed in four steps according to our previously reported procedure.[30] In this process, maltol (**1**) was used as the starting material that reacted with 3-aminobenzoic acid (**2**) to drive the compound (**3**). In the next step, the reaction of compound (**3**) with methanol in the presence of CDI as coupling agent and DMAP led to compound (**4**) in the form of an ester. Subsequently, the reaction proceeded to the desired intermediate with the acyl hydrazide motif (**5**) from the reaction of hydrazine hydrate and the compound (**4**). Eventually, the compound (**5**) was condensed with different aldehydes to yield the final products (**6a–6j**) through a Schiff base reaction (Fig. 2).

2.1.1 Spectra data

*2.1.1.1 Synthesis of methyl 3-(3-hydroxy-2-methyl-4-oxopyridin-1(4H)-yl)benzoate (**4**).* Yield: 42.6%; m.p. 258 °C; IR (KBr, cm^{-1}): 3424, 3080, 3050, 1720, 1626, 1574,1115, 1099; ^{1}H-NMR (300 MHz, DMSO-d_6) δ_H (ppm): 8.13 (s, 1H); 8.00 (s, 1H); 7.73–7.82 (m, 3H); 6.6 (d, 1H); 3.87 (s, 3H); 2 (s, 3H).

*2.1.1.2 Synthesis of 3-(3-hydroxy-2-methyl-4-oxopyridin-1(4H)-yl)benzohydrazide (**5**).* Yield: 84%; m.p. 249 °C; IR (KBr, cm^{-1}): 3329, 3219, 3050, 3020, 1666, 1632, 1576, 1524, 1206, 1096; ^{1}H-NMR (300 MHz, DMSO-d_6) δ_H (ppm): 9.9 (s, 1H); 7.95 (s, 1H); 7.8 (s, 1H); 7.62 (s, 2H); 7.575 (d, 1H); 6.215 (d, 1H); 4.6 (s, 2H); 1.96 (s, 3H).

*2.1.1.3 Synthesis of 3-(3-hydroxy-2-methyl-4-oxopyridin-1(4H)-yl)-N′-(2-nitrobenzylidene)benzohydrazide (**6a**).* Yield: 75%; m.p. 235 °C; IR (KBr, cm^{-1}): 3335, 3200, 3057, 3009, 1693, 1639, 1578, 1549; ^{1}H-NMR (300 MHz, DMSO-d_6) δ_H (ppm):12.35 (brs. 1H, NH), 8.90 (s, 1H), 8.20–8.14 (m, 3H), 8.06 (s, 1H), 7.89 (t, J = 6 Hz, 1H), 7.80–7.79 (m, 2H), 7.69–7.75 (m, 2H), 6.31 (d, J = 6 Hz, 1H), 3.83 (brs, 1H), 2.06 (s, 3H); ^{13}C NMR (75 MHz, DMSO-d_6) δ_C (ppm): 173.25, 162.40, 148.74, 145.57, 144.02, 142.04, 138.41, 134.73, 134.29, 131.33, 131.10, 130.50, 129.07, 128.49, 126.56, 125.19, 111.51, 13.91; MS m/z (%): 392.2 (100).

© 2023 The Author(s). Published by the Royal Society of Chemistry

Open Access Article. Published on 07 November 2023. Downloaded on 2/8/2026 4:49:23 PM.
This article is licensed under a Creative Commons Attribution-NonCommercial 3.0 Unported Licence.

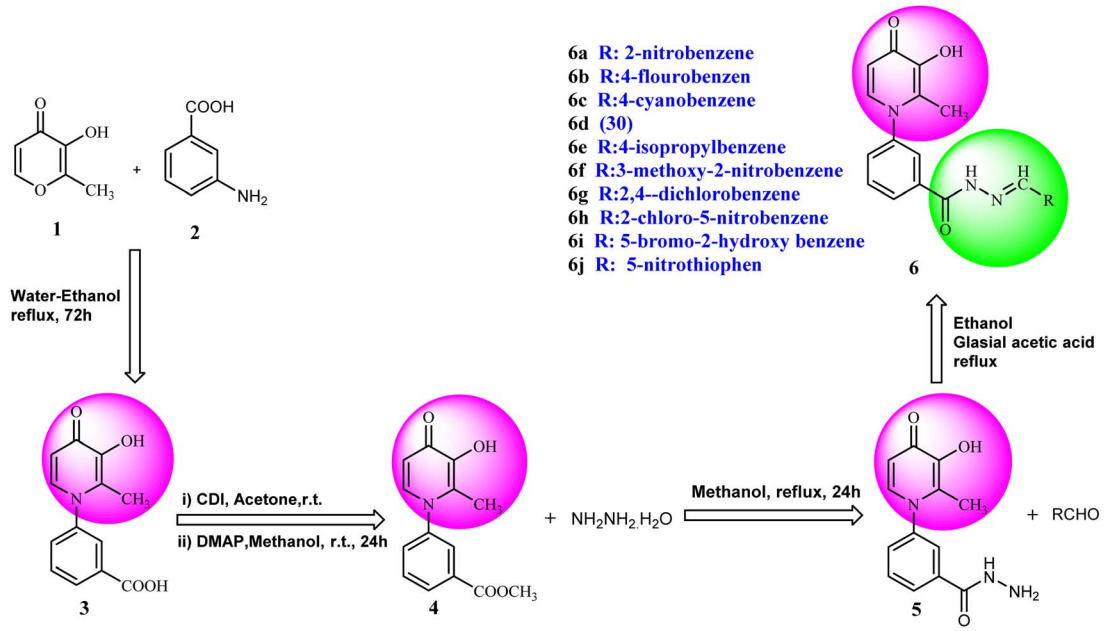

Fig. 2 Outline for the synthesis of 3-hydroxypyridin-4-one derivatives (6a–6j).

*2.1.1.4 Synthesis of 3-(3-hydroxy-2-methyl-4-oxopyridin-1(4H)-yl)-N′-(4-fluorobenzylidene)benzohydrazide (**6b**).* Yield: 67%; m.p. 265 °C; IR (KBr, cm^{-1}): 3354, 3213, 3063, 3038, 1665, 1628, 1603, 1578, 1300; ^{1}H-NMR (300 MHz, DMSO-d_6) δ_H (ppm): 12.04 (s, 1H), 8.56 (s, 1H), 8.14–8.12 (m, 1H), 8.03 (s, 1H), 7.84–7.88 (m, 2H), 7.78 (d, J = 6 Hz, 2H), 7.69 (d, J = 9 Hz, 1H), 7.37 (t, J = 9 Hz, 2H), 6.32 (d, J = 6 Hz, 1H), 3.82 (brs, 1H), 2.06 (s, 3H); ^{13}C NMR (75 MHz, DMSO-d_6) δ_C (ppm): 170.26, 164.92, 145.62, 142.05, 141.98, 138.53, 138.40, 135.15, 130.30, 130.12, 129.09, 128.11, 125.83, 123.89, 122.90, 116.65, 116.29, 111.56, 13.84; MS *m*/*z* (%): 199.1 (97), 365.3 (100).

*2.1.1.5 Synthesis of 3-(3-hydroxy-2-methyl-4-oxopyridin-1(4H)-yl)-N′-(4-cyanobenzylidene)benzohydrazide (**6c**).* Yield: 82.6%; m.p. 205 °C; IR (KBr, cm^{-1}): 3196, 2226, 1670; ^{1}H-NMR (300 MHz, DMSO-d_6) δ_H (ppm): 12.26 (brs, NH); 8.52 (s, 1H); 8.09 (s, 1H); 7.93 (m, 5H); 7.72 (s, 3H); 7.60 (s, 1H), 6.23 (s, 1H); 1.98 (s, 3H); ^{13}C NMR (75 MHz, DMSO-d_6) δ_C (ppm): 170.25, 164.92, 162.42, 146.80, 145.63, 142.04, 139.05, 138.40, 135.18, 134.85, 133.27, 130.53, 130.20, 129.17, 128.19, 126.54, 119.11, 112.52, 111.53, 13.91; MS *m*/*z* (%): 372.2 (80); 244 (26); 226 (36); 199 (100); 154 (17); 128 (44) (100); 77.1 (44); 55.1 (64).

*2.1.1.6 Synthesis of 3-(3-hydroxy-2-methyl-4-oxopyridin-1(4H)-yl)-N′-(4-methylbenzylidene)benzohydrazide (**6d**).* M.p. 330 °C; ref. 30.

*2.1.1.7 Synthesis of 3-(3-hydroxy-2-methyl-4-oxopyridin-1(4H)-yl)-N′-(4-isopropylbenzylidene)benzohydrazide (**6e**).* Yield: 74.3%; m.p. 135 °C; ^{1}H-NMR (300 MHz, DMSO-d_6) δ_H (ppm): 1.26–1.28 (m, 6H); 2.06 (s, 3H); 2.98 (m, 1H); 6.32 (d, J = 9 Hz, 1H); 7.33–7.49 (m, 3H); 7.71–7.87 (m, 4H); 8.03–8.18 (m, 2H); 8.47 (s, 1H); 11.94 (s, 1H); ^{13}C NMR (75 MHz, DMSO-d_6) δ_C (ppm): 170.24, 164.91, 162.07, 153.37, 148.84, 142.62, 142.01, 138.40, 135.23, 135.16, 130.29, 130.12, 129.12, 129.09, 128.12, 127.76, 127.34, 126.42, 125.83, 111.52, 33.87, 24.14, 13.85; MS *m*/*z* (%): 389.2 (49); 355 (18); 292 (13); 249 (28); 221 (33); 149 (100); 105 (62); 71 (43); 43 (68).

*2.1.1.8 Synthesis of 3-(3-hydroxy-2-methyl-4-oxopyridine-1(4H)-yl)-N′-(3-methoxy-2-nitrobenzylidene)benzohydrazide (**6f**).* Yield: 80%; m.p. 189 °C; IR (KBr, cm^{-1}): 3210, 3094, 2990, 2930, 1682, 1630, 1574, 1555, 1533, 1377, 1302, 1202, 1076; ^{1}H-NMR (300 MHz, DMSO-d_6) δ_H (ppm): 12.14 (s, 1H); 8.36 (s, 1H); 8.07 (s, 1H); 7.97 (s, 1H); 7.59–7.78 (m, 5H); 7.43 (d, J = 9 Hz, 1H); 6.22 (d, J = 9 Hz, 1H); 3.93 (s, 3H); 2.00 (s, 3H); ^{13}C NMR (75 MHz, DMSO-d_6) δ_C (ppm): 170.25, 162.18, 150.85, 145.62, 142.05, 141.45, 140.23, 138.39, 134.64, 132.36, 131.18, 130.53, 129.08, 126.52, 118.79, 115.34, 111.54, 57.31, 56.49, 19.02, 13.89; MS *m*/*z* (%): 422.2 (47.9); 244.1 (15); 228.1 (27.4); 200.1 (100); 76.1 (21.3).

*2.1.1.9 Synthesis of 3-(3-hydroxy-2-methyl-4-oxopyridin-1(4H)-yl)-N′-(2,4-dichlorobenzylidene)benzohydrazide (**6g**).* Yield: 55%; m.p. 200 °C; IR (KBr, cm^{-1}): 3300, 3208, 3067, 2924, 1668, 1626, 1433; ^{1}H-NMR (300 MHz, DMSO-d_6) δ_H (ppm): 12.21 (s, 1H), 8.80 (s, 1H), 8.1–8.09 (m, 1H), 8.06–8.03 (m, 1H), 8.00 (s, 1H), 7.75–7.74 (m, 2H), 7.64 (d, 1H, J = 9 Hz), 7.56–7.54 (m, 1H), 6.25 (s, 1H), 2.01 (s, 3H); ^{13}C NMR (75 MHz, DMSO-d_6) δ_C (ppm): 170.27, 162.24, 145.71, 145.35, 142.55, 142.06, 138.39, 135.75, 134.81, 134.42, 131.11, 131.08, 131.01, 130.52, 129.90, 129.04, 128.60, 126.51, 111.52, 13.90; MS *m*/*z* (%): 415.1 (55), 228.1 (30), 199.1 (100), 154.1 (15).

*2.1.1.10 Synthesis of 3-(3-hydroxy-2-methyl-4-oxopyridin-1(4H)-yl)-N′-(2-chloro-5-nitrobenzylidene)benzohydrazide (**6h**).* Yield: 70%; m.p. 316 °C; IR (KBr, cm^{-1}): 3366, 3210, 3050, 1674, 1632, 1611, 1564, 1526, 1342, 1302, 1198, 1045; ^{1}H-NMR (300 MHz, DMSO-d_6) δ_H (ppm):12.38 (s, 1H); 8.83 (s, 1H); 8.695 (s, 1H); 8.23 (dd, J = 15 Hz, J = 3 Hz, 1H); 8.11 (s, 1H); 8.02 (s, 1H); 7.82 (d, 1H J = 15 Hz); 7.76 (s, 2H); 7.65 (d, 1H J = 6 Hz); 6.28 (d, 1H, J = 9 Hz); 2.02 (s, 3H); ^{13}C NMR (75 MHz, DMSO-d_6) δ_C (ppm): 170.25, 162.04, 156.34, 146.01, 145.60, 142.04, 141.66, 138.42, 134.58, 134.24, 131.07, 130.43, 129.12, 126.49, 121.88, 119.14, 111.57, 111.00, 13.93; MS *m*/*z* (%): 331.1 (13.3); 244.1 (81.3); 226.1 (20); 199.1 (42.6); 163.1 (100); 133.1 (14.6); 90.1 (37.3).

© 2023 The Author(s). Published by the Royal Society of Chemistry

Open Access Article. Published on 07 November 2023. Downloaded on 2/8/2026 4:49:23 PM.
This article is licensed under a Creative Commons Attribution-NonCommercial 3.0 Unported Licence.

2.1.1.11 Synthesis of 3-(3-hydroxy-2-methyl-4-oxopyridin-1(4H)-yl)-N′-(5-bromo-2-hydroxybenzylidene)benzohydrazide (6i). Yield: 32%; m.p. 310 °C; IR (KBr, cm^{-1}): 3356, 3213, 3073, 2932, 1684, 1630; ^{1}H-NMR (300 MHz, DMSO-d_6) δ_H (ppm): 12.22 (s, 1H), 8.62 (s, 1H), 8.1 (t, J = 3 Hz, 1H), 8.00 (s, 1H), 7.83 (d, J = 2.6 Hz, 1H), 7.74 (d, J = 3 Hz, 2H), 7.64 (d, J = 9 Hz, 1H), 7.44 (dd, J = 9 Hz, J = 3 Hz, 1H) 6.91 (d, J = 9 Hz, 1H), 6.26 (d, J = 9 Hz, 1H), 2.01 (s, 3H); ^{13}C NMR (75 MHz, DMSO-d_6) δ_C (ppm): 170.23, 162.03, 156.86, 146.07, 145.62, 142.04, 138.41, 134.58, 134.22, 131.05, 130.52, 129.21, 129.07, 126.48, 121.87, 119.14, 111.58, 110.99, 109.30, 13.91; MS *m*/*z* (%): 441.1 (10), 227.1 (100), 201.1 (70), 170.1 (11), 76.1 (12.5).

2.1.1.12 Synthesis of 3-(3-hydroxy-2-methyl-4-oxopyridin-1(4H)-yl)-N′-((5-nitrothiophen-2-yl)methylene)benzohydrazide (6j). Yield: 53%; m.p. 248 °C; ^{1}H-NMR (300 MHz, DMSO-d_6) δ_H (ppm): 12.4 (s, 1H), 8.69 (s, 1H), 8.26–7.98 (m, 4H), 7.62–7.45 (m, 3H), 6.26 (s, 1H), 3.60 (s, 1H), 2.00 (s, 1H). ^{13}C NMR (75 MHz, DMSO-d_6) δ_C (ppm): 186.5, 162.5, 151.5, 146.9, 146.8, 145.6, 142.1, 138.4, 136.2, 134.6, 131.2, 130.9, 130.6, 130.5, 129.1, 126.6, 111.6, 13.9.

2.2 Inhibitory effect of analogs on the activity of mushroom tyrosinase

The tyrosinase inhibitory activity of all synthesized compounds is shown in Table 1. Seven derivatives present an appropriate inhibitory effect with an IC_{50} range of 25.29–64.13 μM compared to kojic acid as the positive control. The compounds **6i** and **6d** revealed the highest activity on tyrosinase inhibition with IC_{50} values of 25.29 and 26.36 μM. In the assessment of the mono-substituted group (**6a–6e**), it can be stated that the presence of an electron-donating group, such as methyl, at the para position of the phenyl moiety, can improve the tyrosinase inhibitor activity, just as the introduction of the electron-withdrawing group (NO_2) in the ortho position showed good activity with an IC_{50} = 28.57 μM. Compounds **6b** and **6e** bearing fluoro and isopropyl groups at C_4 of the phenyl ring also showed appropriate tyrosinase inhibitory activity. Finally, the presence of the cyanide group led to diminished activity (IC_{50} > 100 μM). In the case of di-substitution (**6f–6i**), compound **6i** (R =OH, Br) had the best anti-tyrosinase potency with an IC_{50} = 64.13 μM. The substitution of chloro at the *meta* and *ortho* positions led to significantly decreased activity in compound **6g**. In general, it can be seen that most of the multi-substitution compounds such as **6f**, **6h** bearing R = 2-NO_2, 3-OCH_3 and R = 2-Cl, 5-NO_2 had weak inhibitory activity, and compound **6j** containing 2-nitro thiol ring also had low potential. Taken together, mono-substituted compounds had better diphenolase inhibitory properties than multi-substitution series (**6f–6i**). The SAR study indicated that positioning methyl at a phenyl ring, such as compound **6d**, led to an increase in activity in series 1, and concerning series 2, placing the brome and hydroxyl groups at 2, 5 positions caused improved activity compared to other compounds.

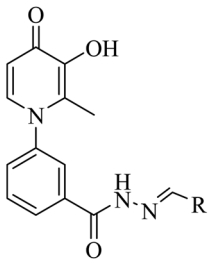

(6a-6j)

Table 1 IC_{50} values for tyrosinase inhibition activity of studied compounds and kojic acid

ID	R	Inhibition%[a] ± SEM[b]	IC_{50}[c] (μM)	ID	R	Inhibition%[a] ± SEM[b]	IC_{50}[c] (μM)
6a	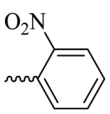	46.07 ± 8.21	28.57	**6f**	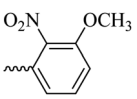	34.83 ± 3.83	>100
6b	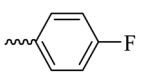	43.08 ± 3.41	33.41	**6g**	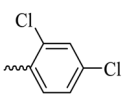	28.14 ± 3.97	43.65
6c	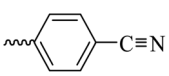	30.84 ± 2.85	>100	**6h**	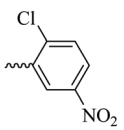	11.38 ± 2.59	>100
6d	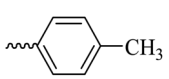	49.04 ± 7.51	26.36	**6i**	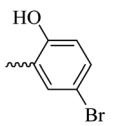	49.63 ± 12.63	25.29
6e	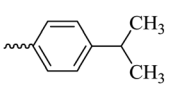	41.69 ± 4.07	34.27	**6j**	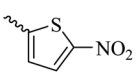	40.35 ± 5.00	64.13
Kojic acid	—	62.67 ± 7.88	16.68				

[a] Values for tested compounds and kojic acid were measured at 50 μM. [b] Values for 3 repetitions of the experiment. [c] 50% inhibitory concentration (IC_{50}).

© 2023 The Author(s). Published by the Royal Society of Chemistry

Open Access Article. Published on 07 November 2023. Downloaded on 2/8/2026 4:49:23 PM.
This article is licensed under a Creative Commons Attribution-NonCommercial 3.0 Unported Licence.

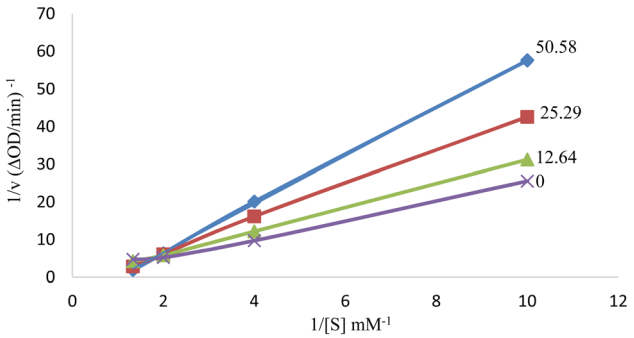

Fig. 3 Lineweaver–Burk plot for tyrosinase enzyme inhibition by different concentrations of **6i** in the presence of L-Dopa (double reciprocal plot, $n = 3$).

2.3 Determination of the inhibition type

The inhibition type on tyrosinase enzyme was determined for the compound **6i** as the best antityrosinase. For consideration of the inhibition type, Lineweaver–Burk plots (plot of $1/V$ *versus* 1/[S]) were drawn with several concentrations of **6i** (as the inhibitor) and L-Dopa (as the substrate).[31] The results showed that the K_m value was increased along with increasing the concentration of inhibitor while V_{max} was not affected by the concentration. According to the obtained results, it can be concluded that compound **6i** acts as the competitive inhibitor of tyrosinase enzyme. It can be assumed that the structural similarity of compound **6i** and the substrate of the mushroom tyrosinase enzyme (L-Dopa), especially the presence of the phenolic group, has caused competition with the substrate to bind to the active site of the enzyme (Fig. 3).[32]

2.4 Free radical scavenging activity

The radical scavenging activity toward DPPH was represented in Table 2 in EC_{50} values. The analogs (**6a**, **6b**, and **6e**) having 2-NO_2, 4-F, and 4-*iso*-propyl moiety were found to have excellent radical scavenging potential with EC_{50} = 0.032, 0.012, and 0.014 mM, respectively. Further investigations demonstrated that the presence of cyanide, methyl, and multi-substitution groups also led to a decrease in activity. The structure–activity relationship revealed that the presence of an electron-donating group, such as isopropyl, and an electron-withdrawing group, such as a fluorine atom, on the phenyl ring caused an improvement in activity, and the existence of a nitro group at the *ortho* position of the phenyl ring increased the DPPH activity.

2.5 Molecular docking study

Molecular docking was used to predict the binding mode and interaction of potent compound (**6i**) in the active site of the tyrosinase enzyme (PDB ID: 2y9x). In the binding pocket of the tyrosinase enzyme, two copper atoms interacted with residues, including His85, His61, and His94 in one subunit and His259, His263, and His296 in another subunit.[33] The copper atoms are

Table 2 EC_{50} value of synthesized compounds in comparison with quercetin

ID	DPPH (%)	EC_{50} (mM)	Compound	DPPH (%)	EC_{50} (mM)
6a	77.15	0.032 ± 0.01	**6f**	43.67	0.168 ± 0.03
6b	71.42	0.012 ± 0.06	**6g**	39.11	0.191 ± 0.07
6c	43.67	0.216 ± 0.08	**6h**	31.91	>400
6d	39.13	0.369 ± 0.01	**6i**	42.64	0.185 ± 0.13
6e	61.44	0.014 ± 0.01	**6j**	42.74	0.383 ± 0.12
Quercetin	74.33	0.0089			

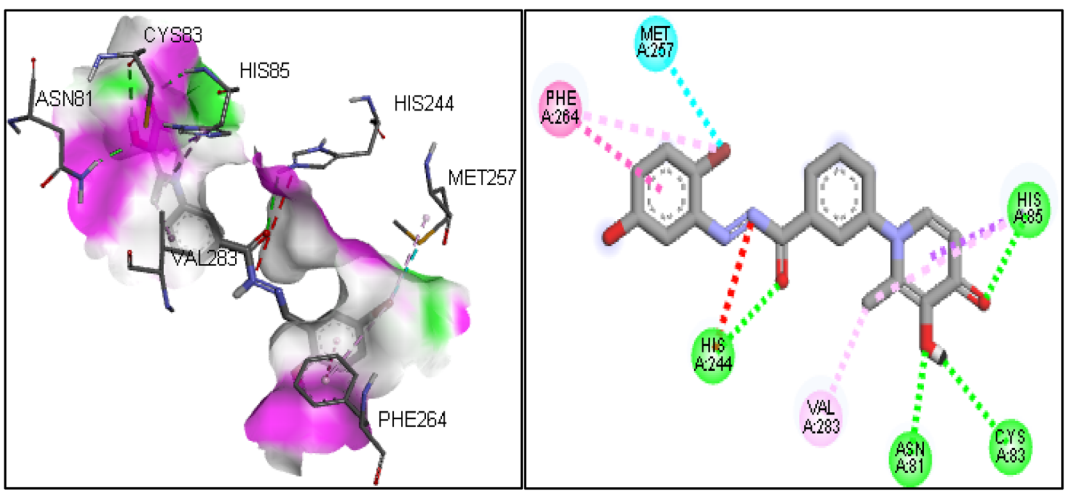

Fig. 4 Interaction and binding mode of compound **6i** in the active site of 2y9x.

Open Access Article. Published on 07 November 2023. Downloaded on 2/8/2026 4:49:23 PM.
This article is licensed under a Creative Commons Attribution-NonCommercial 3.0 Unported Licence.

essential to the enzyme's catalytic activity.[34] If synthesized compounds interact with the residues of copper atoms, they can inhibit the tyrosinase enzyme. The molecular docking results on compound **6i** showed that this compound involved His85 and His244 by hydrogen bonding, which were vital residues in the binding pocket.[35] Also, the hydroxyl group in the 1,4-dihydroxypyridinone ring established a hydrogen bond with residues of Asn81 and Cys83. Another important interaction was the T-shaped interaction with Phe264. The 2D and 3D interactions for compound **6i** are shown in Fig. 4.

2.6 DFT analysis

The DFT analysis calculated the compound **6i** as the best antityrosinase activity and the compound 6 h as one of the compounds with the lowest antityrosinase activity. This analysis is valuable because it predicts the reactivity of compounds in chemical reactions. One of the calculated parameters is the homo, LUMO energies, and the energy gap between them, which is shown for the compounds in Fig. 5. The HOMO–LUMO gap for **6h** and **6i** was obtained at 2.56 ev and 2.99 ev, respectively. As can be seen, the HOMO is on the 3-hydroxypyridine-4-one ring and the LUMO is located on the rest of the molecules for compounds of **6h** and **6i**. The electrostatic potential (ESP) surface or map of compounds is shown in Fig. 6. The negative and positive charge sites are indicated with red and blue colors, respectively. The thermochemical parameters were calculated and are presented in Table 3. The results for the total energy (E), enthalpy (H), and Gibbs free energy (G) showed that compound **6i** is more thermodynamically stable than **6h**. Also according to theoretical calculations, IR spectra for both compounds are depicted in Fig. 7. As it is clear from the spectra of the two compounds, the obtained results confirm the structure of both compounds, which is consistent with the laboratory results.

2.7 *In silico* ADME properties

The physicochemical properties of the studied compounds were obtained using the online software SwissADME. The pharmacokinetic properties of the tested compounds are given in Table 4. For a compound to pass the drug-likeness test, five characteristics of MW $\leq$ 500 Da, log$p$ < 5, nHBD $\leq$ 5, nHBA $\leq$ 10, and TPSA $\leq$ 140 Å must be stated in the range.[36] As observed in Table 4, all compounds were within an acceptable range. In the logK_p parameter (skin permeability), the range of −1 to −8 indicates penetration into the skin, and for our compounds, the values were obtained above −8. In the bioavailability radar shown in the table, the colored zone indicates the suitable physicochemical space for oral bioavailability. It proved that all the synthetic compounds were placed in a suitable space.[37] The results showed that the oral bioavailability of derivatives was good and could be described as "drug-like".

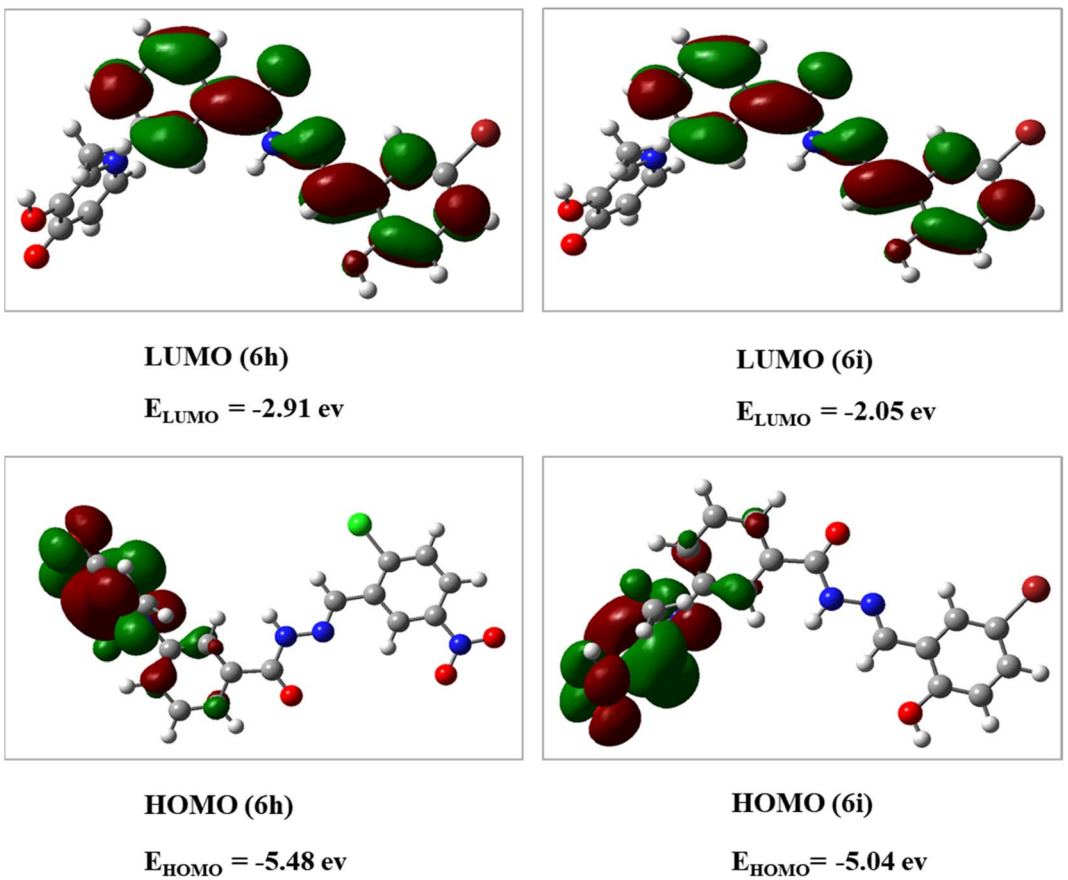

Fig. 5 Calculated LUMO and HOMO for **6h** and **6i** at B3LYP/6-31+G** level of theory.

© 2023 The Author(s). Published by the Royal Society of Chemistry

Open Access Article. Published on 07 November 2023. Downloaded on 2/8/2026 4:49:23 PM.
This article is licensed under a Creative Commons Attribution-NonCommercial 3.0 Unported Licence.

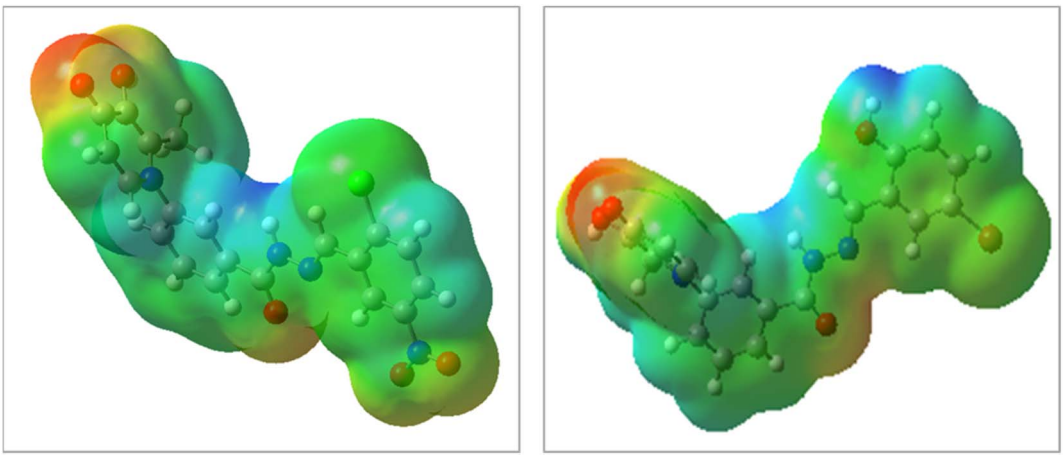

Fig. 6 Electron density maps of **6h** (left) and **6i** (right) at B3LYP/6-31+G** level of theory.

Table 3 The chemical reactivity indices of **6h** and **6i** at B3LYP/6-31+G(d,p) level of theory

Entry	E_{tot} [a]	H [a]	G [a]	S [b]	η [c]	σ [d]	A [c]
6h	−1816.215	−1816.214	−1816.303	186.280	1.282	0.78	2.916
6i	−3791.496	−3791.495	−3791.580	178.766	1.498	0.667	2.052

[a] Hartree per particle. [b] cal mol^{-1} K^{-1}. [c] eV. [d] eV^{-1}

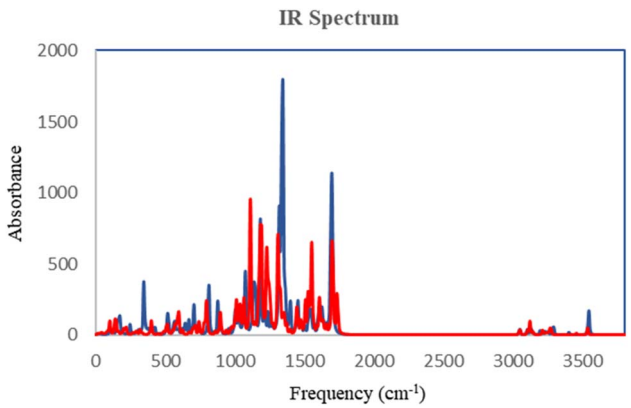

Fig. 7 Calculated IR data for **6h** (red) and **6i** (blue) at B3LYP/6-31+G** level of theory.

3. Material and methods

3.1 Apparatus

All reagents and solvents were purchased from commercial suppliers. Analytical thin layer chromatography (TLC) was performed on MERCK-precoated silica gel 60-F254 (0.5 mm) aluminum plates. Thin layer chromatography (TLC) was used to control the progress of the reaction on MERCK precoated silica gel 60-F254 (0.5 mm) aluminum plates. Melting points were determined on a Kofler hot stage apparatus. The IR spectra were obtained using Nicolet's FT-IR Magna 550 spectrometer (KBr disks). ^{1}H and ^{13}C NMR spectra were recorded on a Bruker 300 MHz NMR instrument using $CDCl_3$ as solvent and TMS as an internal standard. The chemical shifts (δ) and coupling constants (J) are expressed in parts per million (ppm) and hertz (Hz), respectively.

Table 4 Lipinski properties of (**6a–6j**) derivatives

ID	M.W.	nRB	nHBA	nHBD	TPSA	log p	Lipinski rule/violation	log k_p
6a	392.36	6	6	2	129.51	0.71	0	−6.71
6b	365.36	5	5	2	83.69	2.05	0	−7.02
6c	372.38	5	5	2	107.48	1.02	0	−7.33
6d	361.39	5	4	2	83.69	1.89	0	−6.64
6e	389.45	6	4	2	83.69	2.32	0	−6.27
6f	422.39	7	7	2	138.74	0.44	0	−6.91
6g	416.26	5	4	2	83.69	2.64	0	−5.84
6h	426.81	6	6	2	129.51	1.21	0	−6.47
6i	442.26	5	5	3	103.92	1.73	0	−6.65
6j	398.39	6	6	2	157.75	0.29	0	−6.49

Open Access Article. Published on 07 November 2023. Downloaded on 2/8/2026 4:49:23 PM.
This article is licensed under a Creative Commons Attribution-NonCommercial 3.0 Unported Licence.

3.2 Synthesis

3.2.1 General procedure for the synthesis of compound 3-(3-hydroxy-2-methyl-4-oxopyridin-1(4*H*)-yl)-*N*′-benzohydrazide (5). Firstly, maltol (50 mmol) (**1**) was reacted with 3-aminobenzoic acid (50 mmol) (**2**) in a mixture of water and ethanol as solvent at 100 °C for 72 h to obtain compound (**3**). The filtration method was applied to purify the pale-yellow precipitate to give compound (**3**) (43 mmol) (86%, m.p. 265 °C MP).[38] Carbonyldiimidazole (CDI) (9 mmol) was added to the solution of compound (**3**) (5 mmol) in anhydrous acetone (15 mL) and stirred for 1 hour at 25 °C. Then, dimethylaminopyridine (DMAP) (0.5 mmol) was dissolved in 7 mL of anhydrous methanol and added to the mixture, and the stirrer operation continued overnight at room temperature. The completion of the reaction was checked by TLC (5 : 1 chloroform/methanol).[39] Consequently, the mixture was extracted with water and dichloromethane and concentrated to yield the white-colored intermediate[4] (1 mmol) (20%, m.p. 160 °C). The compounds[4] (0.5 mmol) and hydrazine hydrate (1 mmol) in the presence of methanol (5 mL) were reacted under reflux at 90 °C for 24 h. The obtained precipitate was filtered off and washed with cold methanol to furnish compound (**5**) (0.4 mmol) (80%, m.p.247 °C).

3.2.2 General procedure for the synthesis of benzohydrazide derivatives (6a–6j). The anhydrous ethanol (5 mL) and a few drops of glacial acetic acid were poured into the flask containing the mixture of different aldehydes (0.0005 mol), and the mixture was stirred for 15 minutes at 25 °C. During the stirrer, compound **5** (0.5 mmol) in anhydrous ethanol (5 mL) was slowly added dropwise and refluxed at 90–100 °C until the reaction was deemed complete by TLC (methanol/ethyl acetate 3 : 1). The crystalline products isolated by filtration were recrystallized in a desired ratio of ethyl acetate and petroleum ether to give the final products (**6a–6j**) (Fig. 2).

3.3 Enzymatic assay for measurement of tyrosinase inhibition

The assessment of tyrosinase inhibition was measured using L-Dopa as the substrate according to previously reported methods.[40] This method monitors the conversion of L-Dopa to dopachrome at 475 nm. Firstly, the serial dilution of derivatives was prepared and added to tyrosinase dissolved in phosphate buffer (pH = 6.8) in 96-well microplates. Then L-Dopa was added to the mixture after incubation for 20 min. The results were compared to kojic acid as a reference compound. The percentage of inhibition of the proposed compounds was calculated as follows:

$$\%\ \text{Inhibition} = (A_{\text{control}} - A_{\text{sample}}/A_{\text{control}}) \times 100$$

3.4 Determination of the inhibition type

Kinetic analysis was performed on the best compound as anti-tyrosinase activity, **6i**. The concentrations of inhibitor were: 50.58, 25.29, 12.64, and 0 μM. Substrate (L-Dopa) concentrations were 0.5–10.0 mM in all kinetic studies. Determining the type of tyrosinase inhibition was done according to the protocol reported in previous studies. Maximum initial velocity was determined from the initial linear portion of absorbance up to 10 min after the addition of L-Dopa with 1 min interval. The Michaelis constant (K_m) and the maximal velocity (V_{max}) of the tyrosinase activity were determined by the Lineweavere–Burk plot at various concentrations of L-Dopa as a substrate. The inhibition type of the enzyme was evaluated by Lineweavere–Burk plots of the inverse of velocities ($1/V$) *versus* the inverse of substrate concentrations 1/[S] mM^{-1}.

3.5 Enzymatic assay for measurement of antioxidant

The antioxidant assay was evaluated using 1,1-diphenyl-2-picryl hydrazine (DPPH) radical scavenging according to the previously reported method.[41] The decolorization of the DPPH solution after adding the tested compounds as antioxidant agents was measured at 517 nm. The percentage of DPPH radical scavenging activity was calculated as follows:

DPPH radical scavenging, % = $(A_0 - A_s/A_0) \times 100$ where A_0 is the absorbance of the DPPH solution and as is the absorbance of the sample. The results were compared to ascorbic acid as a positive control.

3.6 Molecular docking study

Molecular docking was conducted using AutoDock 4.2 and AutoDock Tools 1.5.4 (ADT).[42] Firstly, the 3D crystal structure of the tyrosinase enzyme complexed with tropolone was downloaded from the protein data bank (**https://www.rcsb.org/**) with PDB ID: 2y9x.[43] Water, ions, and cocrystals were deleted to prepare the receptor file; hydrogens were added; and Gasteiger charges were computed. The designed structures were drawn, minimized using ChemBio 3D, and converted to pdbqt format. The grid box was set with dimensions of 40 × 40 × 40, and docking runs were set at 100. The interaction and binding modes were visualized by the Discovery Studio 2016 client.

3.7 DFT analysis

The density functional theory (DFT) was performed by Gaussian 09 at the B3LYP/6-31+G** level of theory for the compounds of **6h** and **6i**. DFT analysis computed the HOMO and LUMO energies, electron surface potential (ESP), FT-IR vibrational frequencies, and the thermochemistry parameters with B3LYP/6-31+G**.

3.8 *In silico* ADME profile measurement

The studied compounds' pharmacokinetic properties, including absorption, distribution, metabolism, and excretion, were obtained using SWISSADME online software.[44] To determine drug-like and oral bioavailability, parameters of molecular weight, number of hydrogen bonds of acceptors, number of hydrogen bonds of donors, number of rotatable bonds, and TPSA were considered.

© 2023 The Author(s). Published by the Royal Society of Chemistry

Open Access Article. Published on 07 November 2023. Downloaded on 2/8/2026 4:49:23 PM.
This article is licensed under a Creative Commons Attribution-NonCommercial 3.0 Unported Licence.

4. Conclusions

A series of novel 3-hydroxypyridine-4-ones containing benzyl hydrazide with different substitutions were synthesized and assayed as antityrosinase and antioxidant agents. Compound **6i**, containing 5-hydroxyl and 2-bromobenzyl hydrazide motives, had the best anti-tyrosinase activity among all compounds. Also, compound **6b** showed potent activity against antioxidants. The SAR study showed that positioning methyl at the phenyl ring and the brome and hydroxyl groups at the 2, 5 position of phenyl enhanced the activity. In addition, molecular docking analysis revealed that the high tyrosinase inhibitory activity of **6i** may be due to the formation of strong interactions with the critical residues in the active site of the tyrosinase enzyme. The result of the kinetic assay showed a competitive type of inhibition by **6i**. The DFT analysis showed that the HOMO is located on a 3-hydroxypyridin-4-one ring for the studied compounds and also, the compound **6i** as the best antityrosinase compound was thermodynamically stable. Finally, the ADME profile of the proposed compounds proved suitable for bioavailability and drug-likeness. The synthesized compounds can be considered promising leads in tyrosinase studies.

Data availability

The data sets used and analyzed during the current study are available from the corresponding author upon reasonable request. We have presented all data in the form of Tables and Figures. The PDB code (2y9x) was retrieved from the protein data bank (**https://www.rcsb.org/**), **https://www.rcsb.org/structure/2y9x**.

Author contributions

Mehdi Khoshneviszadeh supervised the biological tests. Fateme Zare prepared the manuscript and performed the docking study. Leila Emami wrote the biological part and contributed to the preparation of the manuscript. Bahareh Hassani synthesized the compounds. Razieh Fazel contributed to the synthesis of compounds. Negin Kave performed the biological assay. Razieh Sabet revised the manuscript and edited it. Hossein Sadeghpour supervised the study. All authors read and approved the final manuscript.

Conflicts of interest

The authors declare that they have no competing interests.

Acknowledgements

Financial assistance from the Shiraz University of Medical Sciences through grant numbers 25721 and 24175 is gratefully acknowledged.

References

1 U. Ghani, Carbazole and hydrazone derivatives as new competitive inhibitors of tyrosinase: experimental clues to binuclear copper active site binding, *Bioorg. Chem.*, 2019, **83**, 235–241.
2 N. Fujieda, K. Umakoshi, Y. Ochi, Y. Nishikawa, S. Yanagisawa, M. Kubo, *et al.*, Copper–oxygen dynamics in the tyrosinase mechanism, *Angew. Chem.*, 2020, **132**(32), 13487–13492.
3 D. L. Abd Razak, N. H. M. Fadzil, A. Jamaluddin, N. Y. Abd Rashid, N. A. Sani and M. A. Manan, Effects of different extracting conditions on anti-tyrosinase and antioxidant activities of *Schizophyllum* commune fruit bodies, *Biocatal. Agric. Biotechnol.*, 2019, **19**, 101116.
4 J. Li, L. Feng, L. Liu, F. Wang, L. Ouyang, L. Zhang, *et al.*, Recent advances in the design and discovery of synthetic tyrosinase inhibitors, *Eur. J. Med. Chem.*, 2021, **224**, 113744.
5 S. Y. Lee, N. Baek and T.-g Nam, Natural, semisynthetic and synthetic tyrosinase inhibitors, *J. Enzyme Inhib. Med. Chem.*, 2016, **31**(1), 1–13.
6 S. Karimian, S. Ranjbar, M. Dadfar, M. Khoshneviszadeh, M. Gholampour, A. Sakhteman, *et al.*, 4*H*-benzochromene derivatives as novel tyrosinase inhibitors and radical scavengers: synthesis, biological evaluation, and molecular docking analysis, *Mol. Diversity*, 2021, **25**, 2339–2349.
7 S. Karimian, F. Kazemi, M. Attarroshan, M. Gholampour, S. Hemmati, A. Sakhteman, *et al.*, Design, synthesis, and biological evaluation of symmetrical azine derivatives as novel tyrosinase inhibitors, *BMC Chem.*, 2021, **15**, 1–11.
8 M. Hajimiri, M. Khosravikia, M. Khoshneviszadeh, K. Pedrood, S. Z. Hosseini, M. S. Asgari, *et al.*, Rational design, synthesis, *in vitro*, and *in silico* studies of chlorophenylquinazolin-4 (3*H*)-one containing different aryl acetohydrazides as tyrosinase inhibitors, *Chem. Biodiversity*, 2022, **19**(7), e202100964.
9 Y. T. Wen, Y. Q. Liang, W. M. Chai, Q. M. Wei, Z. Y. Yu and L. J. Wang, Effect of ascorbic acid on tyrosinase and its anti-browning activity in fresh-cut Fuji apple, *J. Food Biochem.*, 2021, **45**(12), e13995.
10 K. Hałdys and R. Latajka, Thiosemicarbazones with tyrosinase inhibitory activity, *MedChemComm*, 2019, **10**(3), 378–389.
11 H. K. Lee, J. W. Ha, Y. J. Hwang and Y. C. Boo, Identification of L-cysteinamide as a potent inhibitor of tyrosinase-mediated dopachrome formation and eumelanin synthesis, *Antioxidants*, 2021, **10**(8), 1202.
12 Y. Matoba, K. Oda, Y. Muraki and T. Masuda, The basicity of an active-site water molecule discriminates between tyrosinase and catechol oxidase activity, *Int. J. Biol. Macromol.*, 2021, **183**, 1861–1870.
13 X. Zhai, R. A. Ward, P. Doig and A. Argyrou, Insight into the therapeutic selectivity of the irreversible EGFR tyrosine kinase inhibitor osimertinib through enzyme kinetic studies, *Biochemistry*, 2020, **59**(14), 1428–1441.

© 2023 The Author(s). Published by the Royal Society of Chemistry

Open Access Article. Published on 07 November 2023. Downloaded on 2/8/2026 4:49:23 PM. This article is licensed under a Creative Commons Attribution-NonCommercial 3.0 Unported Licence.

14 D.-F. Li, P.-P. Hu, M.-S. Liu, X.-L. Kong, J.-C. Zhang, R. C. Hider, *et al.*, Design and synthesis of hydroxypyridinone-L-phenylalanine conjugates as potential tyrosinase inhibitors, *J. Agric. Food Chem.*, 2013, **61**(27), 6597–6603.

15 P. García-Molina, F. García-Molina, J. A. Teruel-Puche, J. N. Rodríguez-López, F. García-Cánovas and J. L. Muñoz-Muñoz, Considerations about the kinetic mechanism of tyrosinase in its action on monophenols: a review, *Mol. Catal.*, 2022, **518**, 112072.

16 J. Tang, H. T. Do, A. D. Huber, M. C. Casey, K. A. Kirby, D. J. Wilson, *et al.*, Pharmacophore-based design of novel 3-hydroxypyrimidine-2,4-dione subtypes as inhibitors of HIV reverse transcriptase-associated RNase H: tolerance of a nonflexible linker, *Eur. J. Med. Chem.*, 2019, **166**, 390–399.

17 J. P. Holt-Martyn, R. Chowdhury, A. Tumber, T. L. Yeh, M. I. Abboud, K. Lippl, *et al.*, Structure-activity relationship and crystallographic studies on 4-hydroxypyrimidine HIF prolyl hydroxylase domain inhibitors, *ChemMedChem*, 2020, **15**(3), 270–273.

18 P. Shirvani, N. Fayyazi, S. Van Belle, Z. Debyser, F. Christ, L. Saghaie, *et al.*, Design, synthesis, *in silico* studies, and antiproliferative evaluations of novel indolin-2-one derivatives containing 3-hydroxy-4-pyridinone fragment, *Bioorg. Med. Chem. Lett.*, 2022, 128784.

19 S. Chaves, L. Piemontese, A. Hiremathad and M. A. Santos, Hydroxypyridinone derivatives: a fascinating class of chelators with therapeutic applications-an update, *Curr. Med. Chem.*, 2018, **25**(1), 97–112.

20 K. Chen, L.-L. Shao, Y.-F. Huo, J.-M. Zhou, Q. Zhu, R. C. Hider, *et al.*, Antimicrobial and antioxidant effects of a hydroxypyridinone derivative containing an oxime ether moiety and its application in shrimp preservation, *Food Control*, 2019, **95**, 157–164.

21 Z. Zarrabi, L. Saghaie, A. Fassihi, N. Pestechian and S. Saberi, Synthesis and comparison of anti-leishmania major activity of antimony and iron complexes of 3-hydroxypyran-4-one and 3-hydroxypyridine-4-one as bi-dentate ligands, *J. Rep. Pharm. Sci.*, 2020, **9**(2), 177.

22 C. Zhang, K. Yang, S. Yu, J. Su, S. Yuan, J. Han, *et al.*, Design, synthesis and biological evaluation of hydroxypyridinone-coumarin hybrids as multimodal monoamine oxidase B inhibitors and iron chelates against Alzheimer's disease, *Eur. J. Med. Chem.*, 2019, **180**, 367–382.

23 H. Sadeghi-Aliabadi, M. A. Zanjanchi, L. Saghaie and M. Borzoei, Evaluation of the cytotoxic effect of hydroxypyridinone derivatives on HCT116 and SW480 colon cancer cell lines, *Pharm. Chem. J.*, 2019, **53**(5), 388–391.

24 L. R. Singh, Y.-L. Chen, Y.-Y. Xie, W. Xia, X.-W. Gong, R. C. Hider, *et al.*, Functionality study of chalcone-hydroxypyridinone hybrids as tyrosinase inhibitors and influence on anti-tyrosinase activity, *J. Enzyme Inhib. Med. Chem.*, 2020, **35**(1), 1562–1567.

25 Y.-Z. Zhu, K. Chen, Y.-L. Chen, C. Zhang, Y.-Y. Xie, R. C. Hider, *et al.*, Design and synthesis of novel stilbene-hydroxypyridinone hybrids as tyrosinase inhibitors and their application in the anti-browning of freshly-cut apples, *Food Chem.*, 2022, **385**, 132730.

26 W. Xia, K. Chen, Y. Z. Zhu, C. J. Zhang, Y. L. Chen, F. Wang, *et al.*, Antioxidant and anti-tyrosinase activity of a novel stilbene analogue as an anti-browning agent, *J. Sci. Food Agric.*, 2022, **102**(9), 3817–3825.

27 D.-Y. Zhao, M.-X. Zhang, X.-W. Dong, Y.-Z. Hu, X.-Y. Dai, X. Wei, *et al.*, Design and synthesis of novel hydroxypyridinone derivatives as potential tyrosinase inhibitors, *Bioorg. Med. Chem. Lett.*, 2016, **26**(13), 3103–3108.

28 L.-L. Shao, X.-L. Wang, K. Chen, X.-W. Dong, L.-M. Kong, D.-Y. Zhao, *et al.*, Novel hydroxypyridinone derivatives containing an oxime ether moiety: synthesis, inhibition on mushroom tyrosinase and application in anti-browning of fresh-cut apples, *Food Chem.*, 2018, **242**, 174–181.

29 Z. Dehghani, M. Khoshneviszadeh, M. Khoshneviszadeh and S. Ranjbar, Veratric acid derivatives containing benzylidene-hydrazine moieties as promising tyrosinase inhibitors and free radical scavengers, *Bioorg. Med. Chem.*, 2019, **27**(12), 2644–2651.

30 R. Sabet, A. Fassihi, B. Hemmateenejad, L. Saghaei, R. Miri and M. Gholami, Computer-aided design of novel antibacterial 3-hydroxypyridine-4-ones: application of QSAR methods based on the MOLMAP approach, *J. Comput. -Aided Mol. Des.*, 2012, **26**, 349–361.

31 S. Nie, F. Wu, J. Wu, X. Li, C. Zhou, Y. Yao, *et al.*, Structure-activity relationship and antitumor activity of 1,4-pyrazine-containing inhibitors of histone acetyltransferases P300/CBP, *Eur. J. Med. Chem.*, 2022, **237**, 114407.

32 I. Kubo and I. Kinst-Hori, Tyrosinase inhibitors from anise oil, *J. Agric. Food Chem.*, 1998, **46**(4), 1268–1271.

33 A. Iraji, T. Adelpour, N. Edraki, M. Khoshneviszadeh, R. Miri and M. Khoshneviszadeh, Synthesis, biological evaluation and molecular docking analysis of vaniline–benzylidenehydrazine hybrids as potent tyrosinase inhibitors, *BMC Chem.*, 2020, **14**(1), 1–11.

34 S. Zolghadri, A. Bahrami, M. T. Hassan Khan, J. Munoz-Munoz, F. Garcia-Molina, F. Garcia-Canovas, *et al.*, A comprehensive review on tyrosinase inhibitors, *J. Enzyme Inhib. Med. Chem.*, 2019, **34**(1), 279–309.

35 R. Fazel, B. Hassani, F. Zare, H. Jokar Darzi, M. Khoshneviszadeh, A. Poustforoosh, *et al.*, Design, synthesis, *in silico* ADME, DFT, molecular dynamics simulation, anti-tyrosinase, and antioxidant activity of some of the 3-hydroxypyridin-4-one hybrids in combination with acylhydrazone derivatives, *J. Biomol. Struct. Dynam.*, 2023, 1–11.

36 C. A. Lipinski, Lead-and drug-like compounds: the rule-of-five revolution, *Drug Discovery Today: Technol.*, 2004, **1**(4), 337–341.

37 K. M. Al Azzam, E.-S. Negim and H. Y. Aboul-Enein, ADME studies of TUG-770 (a GPR-40 inhibitor agonist) for the treatment of type 2 diabetes using SwissADME predictor: *in silico* study, *J. Appl. Pharm. Sci.*, 2022, **12**(4), 159–169.

38 C. Gasche, T. Ahmad, Z. Tulassay, D. C. Baumgart, B. Bokemeyer, C. Büning, *et al.*, Ferric maltol is effective in correcting iron deficiency anemia in patients with

 © 2023 The Author(s). Published by the Royal Society of Chemistry

Open Access Article. Published on 07 November 2023. Downloaded on 2/8/2026 4:49:23 PM.
This article is licensed under a Creative Commons Attribution-NonCommercial 3.0 Unported Licence.

inflammatory bowel disease: results from a phase-3 clinical trial program, *Inflamm. Bowel Dis.*, 2015, **21**(3), 579–588.

39 G. Kontoghiorghes, Chelators affecting iron absorption in mice, *Arzneim. Forsch.*, 1990, **40**(12), 1332–1335.

40 Ş. Akın, E. A. Demir, A. Colak, Y. Kolcuoglu, N. Yildirim and O. Bekircan, Synthesis, biological activities and molecular docking studies of some novel 2,4,5-trisubstituted-1,2,4-triazole-3-one derivatives as potent tyrosinase inhibitors, *J. Mol. Struct.*, 2019, **1175**, 280–286.

41 Z. Peng, Y. Li, L. Tan, L. Chen, Q. Shi, Q.-H. Zeng, *et al.*, Anti-tyrosinase, antioxidant and antibacterial activities of gallic acid-benzylidenehydrazine hybrids and their application in preservation of fresh-cut apples and shrimps, *Food Chem.*, 2022, **378**, 132127.

42 H. Syahputra, M. Masfria, P. Hasibuan and I. Iksen, In silico docking studies of phytosterol compounds selected from *Ficus religiosa* as potential chemopreventive agent, *Rasayan J. Chem.*, 2022, **15**(2), 1080–1084.

43 A. Moulishankar and K. Lakshmanan, Data on molecular docking of naturally occurring flavonoids with biologically important targets, *Data Brief*, 2020, **29**, 105243.

44 M. Abdullahi and S. E. Adeniji, *In silico* molecular docking and ADME/pharmacokinetic prediction studies of some novel carboxamide derivatives as anti-tubercular agents, *Chem. Afr.*, 2020, **3**(4), 989–1000.